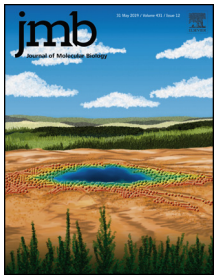

Near Saturation of Ribosomal L7/L12 Binding Sites with Ternary Complexes in Slowly Growing *E. coli*

Mainak Mustafi and James C. Weisshaar

Department of Chemistry, *University of Wisconsin-Madison, Madison, WI 53706, USA*

Correspondence to James C. Weisshaar: *weisshaar@chem.wisc.edu*
https://doi.org/10.1016/j.jmb.2019.04.037
Edited by Anna Pyle

Abstract

For *Escherichia coli* growing rapidly in rich medium at 37 °C, the doubling time can be as short as ~20 min and the average rate of translation (k_{trl}) can be as fast as ~20 amino acids/s. For slower growth arising from poor nutrient quality or from higher growth osmolality, k_{trl} decreases significantly. In earlier work from the Hwa lab, a simplified Michaelis–Menten model suggested that the decrease in k_{trl} arises from a shortage of ternary complexes (TCs) under nutrient limitation and from slower diffusion of TCs under high growth osmolality. Here we present a single-molecule tracking study of the diffusion of EF-Tu in *E. coli* growing with doubling times in the range 62–190 min at 37 °C due to nutrient limitation, high growth osmolality, or both. The diffusive properties of EF-Tu remain quantitatively indistinguishable across all growth conditions studied. Dissection of the total population into ribosome-bound and free sub-populations, combined with copy number estimates for EF-Tu and ribosomes, indicates that in all cases ~3.7 EF-Tu copies are bound on average to each translating 70S ribosome. Thus, the four L7/L12 binding sites adjacent to the ribosomal A-site in *E. coli* are essentially saturated with TCs in all conditions, facilitating rapid testing of aminoacyl-tRNAs for a codon match. Evidently, the average translation rate is not limited by either the supply of cognate TCs under nutrient limitation or by the diffusion of free TCs at high osmolality. Some other step or steps must be rate limiting for translation in slow growth.

Introduction

Bacterial cells including *Escherichia coli* are remarkable for their ability to survive and grow under a wide range of environmental conditions [1–5]. A fundamental quantity closely related to growth rate is the average rate of protein synthesis by translating 70S ribosomes, defined as the mean rate of amino acid incorporation into the growing polypeptide chain (here k_{trl}, in aa/s). The translation elongation cycle comprises a complex series of molecular level events including binding of a ternary complex (TC) to an L7/L12 tether adjacent to the ribosomal A-site; testing of the aminoacyl-tRNA (aa-tRNA) at the A-site for a codon match; rejection and dissociation of non-matching TCs; formation of a new peptide bond to the correct amino acid; and translocation of the tRNAs through the ribosomal A-, P-, and E-sites [6,7]. Each TC contains an aa-tRNA, the translation elongation factor EF-Tu, and GTP. For *E. coli*, many rate constants for individual steps of the elongation cycle have been elucidated by careful kinetic studies *in vitro*, both in bulk and at the single molecule level [7–10]. Detailed kinetics models that are consistent with observed average translation rates *in vivo* have been developed [11,12]. In addition, models incorporating codon-specific elongation rates have been proposed to help explain the effects of depletion of specific TCs under external perturbations [13].

Two important environmental stresses that can severely hinder bacterial growth are nutrient limitation and hyperosmotic stress. In a comprehensive series of papers, Hwa and coworkers have made detailed measurements of the factors governing k_{trl} in live *E. coli* over a wide range of growth rates [14–16]. They explored the effects of nutrient limitation and hyperosmotic stress on the overall growth rate λ, on k_{trl}, on the fraction of the proteome dedicated to ribosomal proteins, on the copy number of the elongation factor EF-Tu relative to that of ribosomes, on the fraction of

ribosomes actively carrying out translation, and on the fraction of tRNA copies charged as aa-tRNA. Remarkably, the data under nutrient limitation [14] with doubling times ranging from 23 min to 20 h fit a simplified, coarse-grained Michaelis–Menten model involving the cognate TC as substrate and the ribosome as enzyme:

$$\frac{1}{k_{trl}} = \frac{1}{k_{on} \times [TC_{eff}]} + \frac{1}{k_{elong}} \quad (1)$$

Here k_{on} (M^{-1} s^{-1}) is the bimolecular rate constant for binding of cognate TCs to the ribosomal A-site (assumed to be diffusion limited), $[TC_{eff}]$ is the concentration of cognate TCs, and k_{elong} (s^{-1}) is the composite rate of all subsequent steps in peptide synthesis. As nutrient quality decreases, the growth rate slows down and the fraction of protein synthesis dedicated to ribosomal proteins decreases. Synthesis of EF-Tu and ribosomal proteins are co-regulated; the ratio of total EF-Tu to ribosomes always lies in the range 6–7 [14–18]. Accordingly, the falloff in k_{trl} as growth rate decreases was judged to arise primarily from a decrease in $[TC_{eff}]$, that is, from limitations on the substrate concentration, with k_{on} and k_{elong} remaining essentially constant. Sub-lethal doses of the translation inhibitor chloramphenicol (Cm) were also used in order to vary $[TC_{eff}]$ under fixed nutrient conditions. This enhances the fraction of proteins dedicated to ribosomes, and the TC and aa-tRNA concentrations increase proportionally. The Cm data fell on the same Michaelis–Menten plot.

In a more recent study [16], the same quantities were measured using glucose as carbon source in minimal Mops-buffered medium (MBM) while varying the overall concentration of the impermeable osmolite NaCl in the medium. As the NaCl concentration increased from 0.1 to 0.6 M, the doubling time at 37 °C varied from 43 to 346 min. At each of two elevated NaCl concentrations 0.3 and 0.4 M, the effective substrate concentration $[TC_{eff}]$ was varied at fixed osmolality by addition of sublethal concentrations of Cm. Lineweaver–Burke plots of k_{trl}^{-1} *versus* $[TC_{eff}]^{-1}$ then indicated that while the maximum elongation rate k_{elong} remained fairly constant with increasing osmolality (22–25 aa/s), the binding rate constant k_{on} decreased by a factor of 2.3, from 6.4×10^6 M^{-1} s^{-1} at 0.1 M NaCl to 2.8×10^6 M^{-1} s^{-1} at 0.4 M NaCl. This decrease was attributed to slower diffusion of TCs in the more crowded cytoplasm at higher osmolality. In summary, Hwa and coworkers conclude that the decrease in overall translation rate under nutrient limitation arises primarily from the scarcity of TCs. The decrease at higher osmolarity arises primarily from increased cytoplasmic crowding, which limits the diffusion coefficient of TCs and thus k_{on}.

We recently reported a single-molecule tracking study of the diffusion of EF-Tu in live *E. coli* growing in EZ-rich defined medium (EZRDM) at 30 °C (doubling time 60 min) [19]. Analysis of the diffusive trajectories enabled us to distinguish two EF-Tu subpopulations: a slowly diffusing component assigned to EF-Tu copies within TCs bound to translating ribosomes and a more rapidly diffusing component assigned as a composite of free EF-Tu copies and free TCs (not bound to ribosomes). For the ribosome-bound sub-population, the localization uncertainty $\sigma \sim 40$ nm makes the method insensitive to the internal motion of an EF-Tu copy tethered to an L7/L12 site. The measurements are only sensitive to the overall movement through space of the ribosome-bound EF-Tu, whether the TC is tethered to L7/L12 or more firmly accommodated within the A-site. From the fractions of slow and fast diffusive components and the known ratio of 6–7 EF-Tu copies per ribosome, we inferred that on average, approximately 4 TCs are bound to each translating ribosome. Before an aa-tRNA can be tested at the A-site, its TC binds to the CTD of an L7/L12 ribosomal subunit (schematic in Fig. 1a) [20–24]. In *E. coli*, four such L7/L12 subunits protrude from the ribosomal stalk adjacent to the A-site [20]. Our quantitative estimate thus indicated that the four L7/L12 subunits are essentially saturated with TCs in moderately good growth conditions at 30 °C. The presence of four TCs on flexible linkers near the A-site presumably facilitates rapid testing of new TCs for a codon match [20].

In view of Hwa's work, here we extend our studies of EF-Tu diffusion to include slower growth (doubling times 62–190 min) at 37 °C arising from the effects of either nutrient limitation or hyperosmotic conditions or both. The diffusion coefficients of fast and slow EF-Tu copies remain quite similar under all conditions studied. In all cases, the data indicate that the four L7/L12 sites remain essentially saturated with TCs. Evidently, neither the concentration of TCs under nutrient limitation nor the diffusion coefficient of TCs in hyperosmotic conditions limits the overall translation rate.

Results

Comparison of EF-Tu/TC diffusion under different osmotic conditions

We used the superresolution technique of photoactivated localization microscopy [25] and single-particle tracking [26] to probe the diffusion of EF-Tu in *E. coli* under various growth conditions having different translation elongation rates. EF-Tu is an essential protein. The background, wild-type (WT) strain is *E. coli* NCM3722. We used a modified strain

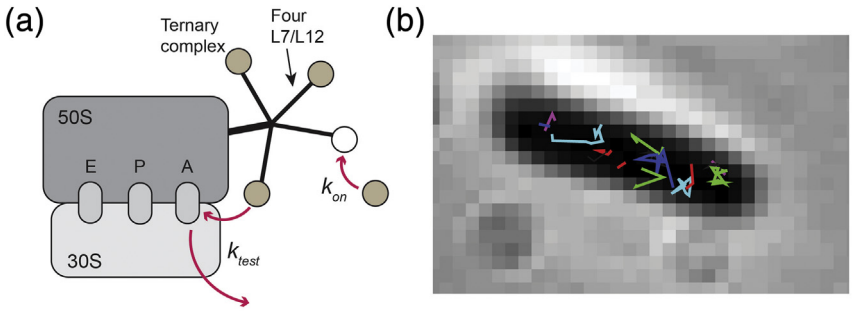

Fig. 1. (a) Schematic diagram of TCs binding to the four L7/L12 ribosomal sites prior to codon testing at the A-site. Because most of the TCs are not cognate, these experiments pertain to the preponderance of events in which a TC binds and is tested and rejected. This must be very rapid to enable delivery of (the unusual) cognate TCs at ~20 aa/s or even faster. (b) EF-Tu/TC trajectories overlaid on the phase contrast image of a cell grown in MBM-glucose with 0.1 M NaCl at 37 °C.

in which the C-termini of the two genes encoding EF-Tu, *tufA* and *tufB* [27], are both fused within the chromosome to the gene expressing the photoconvertible fluorescent protein mEos2. Thus, all expressed copies carry the mEos2 label.

To vary the growth rate and also the elongation rate, we have grown cells in Mops-based minimal growth medium (MBM) with glucose or acetate as the carbon source and with varying osmolality, ranging from 0.28 to 0.81 Osm. The osmolality was varied by including different concentrations of NaCl (0.1 and 0.4 M) in the growth medium. Cells were grown at 37 °C. Under these growth conditions, the doubling time varied from 62 to 190 min (Table S1). The doubling time for the WT strain growing in glucose and 0.28 Osm at 37 °C is 48 min compared to 62 min for the labeled strain. The labeling increases the doubling time by ~30%, a moderate growth defect. The growth curves for the different conditions are shown in Fig. S1. The only phenotypical change observed for the different growth conditions is a decrease in the mean cell length with decreasing growth rate (Fig. S2).

The superresolution imaging experiments yield trajectories of the labeled EF-Tu molecules. EF-Tu may occur as freely diffusing bare EF-Tu, EF-Tu within freely diffusing TCs, or EF-Tu within TCs bound to translating 70S ribosomes. The diffusion of free EF-Tu-mEos2 (~69 kDa) [28,29] and free TC-mEos2 (~93 kDa) are not readily distinguished from one another by short trajectories having significant localization error. Thus, we refer to these two populations combined as "fast EF-Tu." A free protein of similar size should have a diffusion coefficient in the range 4–8 $\mu m^2/s$ [30,31]. Accordingly, we recently reported the diffusion coefficient of the fast EF-Tu population to be $D_{fast} = 4.9 \pm 1.2\ \mu m^2/s$ for VH1000 cells growing in EZRDM at 30 °C [19]. The 70S ribosome/polysome complexes are much larger than a TC (~2.5 MDa for each 70S ribosome) [32,33]. The diffusion coefficient of ribosome-bound TCs should be the same as that of the 70S-polysomes, $\sim 0.3\ \mu m^2/s$ [19,34,35]. This population is referred to as "slow EF-Tu." By modeling the distribution of single-step displacements, we obtain quantitative estimates of the fractional populations of fast and slow states of EF-Tu in each growth condition.

We imaged the EF-Tu-mEos2 molecules in a widefield epifluorescence mode. Only a small subset of fluorophores (~1/frame) were activated using a weak 405-nm laser and those molecules were subsequently excited by a 561-nm laser to observe their fluorescence. The locations of these molecules were recorded and then connected over successive frames to form trajectories. The mean trajectory length was ~3 steps. Imaging was carried out at the fast rate of 2 ms/frame with continuous laser illumination, in order to capture slow and fast EF-Tu copies with similar efficiency. For each of the conditions studied, we analyzed between 1400 and 2100 trajectories of six steps or longer duration. These trajectories were truncated at the sixth step.

We first present a detailed quantitative analysis of EF-Tu diffusion and fractional binding to translating ribosomes for cells grown in MBM glucose medium with 0.1 M NaCl. There follows a comparison of the results across different growth media.

MBM-glucose growth medium with 0.1 M NaCl

The mean diffusion coefficient D_{Mean} of EF-Tu in each growth condition is obtained from the mean-square displacement (MSD) plot *versus* lag time (Fig. 2a). In our previous study of the VH1000 strain grown in the moderately rich growth medium EZRDM at 30 °C [19], we obtained $D_{Mean} = 2.02 \pm 0.19\ \mu m^2/s$, a useful reference number. The present study at 37 °C finds only minor differences in D_{Mean} across the different growth conditions (Table 1). In particular, $D_{Mean} = 1.84 \pm 0.19\ \mu m^2/s$ for

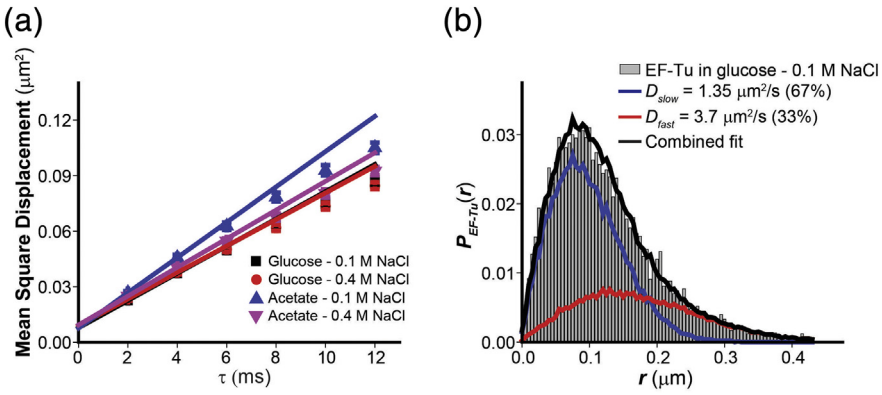

Fig. 2. (a) MSD *versus* τ plot of EF-Tu/TC in different growth media at 37 °C as indicated. The mean diffusion coefficient D_{Mean} as estimated from the slope of the first two points is quite similar in all the different growth conditions studied (Table 1). (b) Histogram of the normalized single-step length distribution of EF-Tu/TC in MBM-glucose with 0.1 M NaCl at 37 °C. Best-fit two-state model results are shown. See Table 1, Materials and Methods, and SI for details.

MBM-glucose with 0.1 M NaCl. In each case, the intercept of the MSD plot yields an estimate of the localization error σ, which is typically ~60 nm.

To study the binding of EF-Tu to ribosomes, we used the same set of six-step trajectories to form a histogram of the distribution of single-step displacements between camera frames, with each step corresponding to a time delay of $\Delta t = 2$ ms. The resulting distribution is normalized to obtain $P_{EF\text{-}Tu}(r)$, as shown in Fig. 2b for cells growing in MBM-glucose with 0.1 M NaCl. To analyze this distribution as a sum of contributions from fast and slow EF-Tu copies, we simulate large sets of random walk trajectories in a confining volume, which matches the dimensions of an average *E. coli* cell growing in each specific growth condition. Each set uses a particular diffusion coefficient D and includes appropriate localization error, as judged from the intercept of the MSD plot. Each value of D yields a simulated numerical distribution of single-step displacements $P_{model}(r, D)$. These serve as basis functions for two-state fitting of the experimental $P_{EF\text{-}Tu}(r)$ in a least-squares sense. We combine pairs of these simulated distributions representing the fast (D_{fast}) and slow (D_{slow}) populations in varied fractions (f_{slow} and $f_{fast} = 1 - f_{slow}$) to determine the best numerical fit to the experimental $P_{EF\text{-}Tu}(r)$ distribution. The goodness of fit is judged by the reduced chi-square statistic, χ^2_ν. For each growth condition, we generate a three-dimensional grid of χ^2_ν values for different choices of D_{slow}, D_{fast} and f_{slow}. The parameters which give the minimum χ^2_ν are chosen as our best-fit parameters. The procedure is explained in more detail in Materials and Methods and in Refs. [19,34].

For MBM-glucose with 0.1 M NaCl, this procedure yields the best-fit values

$D_{slow} = 1.35 \pm 0.30$ μm²/s, $D_{fast} = 3.7 \pm 1.1$ μm²/s, and $f_{slow} = 0.67 \pm 0.05$, with $\chi^2_\nu = 1.07$

(Table 1). The uncertainties are estimated from the range of parameter values that would increase χ^2_ν by 0.5 from its best-fit value. These results are very similar to those obtained earlier for the strain VH1000 in EZRDM at 30 °C [19]. In that case, we obtained the values $D_{slow} = 1.0 \pm 0.2$ μm²/s, $D_{fast} = 4.9 \pm 1.2$ μm²/s, and $f_{slow} = 0.60 \pm 0.05$. One-state fitting to the same data yields only very poor fits; the best value of χ^2_ν was 4.8 (SI, Table S3). We also explored three-state fitting of the same $P_{EF\text{-}Tu}(r)$ distribution with D_{slow} constrained to the ribosome value of 0.3 μm²/s and D_{medium}, D_{fast} and the fractional populations f_{slow} and f_{medium} as adjustable parameters, making a four-dimensional search grid. This

Table 1. Results of two-state fitting of EF-Tu diffusion for four different growth conditions

Growth medium[a]	Osmolality (Osm)	Doubling time (min)	D_{Mean}[b] (μm²/s)	D_{fast}[c] (μm²/s)	D_{slow}[c] (μm²/s)	f_{slow}[c]	χ^{2c}_ν
Glucose–0.1 M NaCl	0.28	62 ± 2	1.84 ± 0.19	3.7 ± 1.1	1.35 ± 0.30	0.67 ± 0.05	1.07
Glucose–0.4 M NaCl	0.81	104 ± 4	1.79 ± 0.16	3.5 ± 1.0	1.0 ± 0.1	0.65 ± 0.05	1.28
Acetate–0.1 M NaCl	0.3	101 ± 2	2.38 ± 0.21	4.3 ± 0.9	1.5 ± 0.3	0.55 ± 0.05	0.95
Acetate–0.4 M NaCl	0.81	190 ± 9	1.94 ± 0.16	4.1 ± 0.6	1.65 ± 0.20	0.65 ± 0.05	1.15
EZRDM 30 °C	0.28	60 ± 3	2.02 ± 0.19	4.9 ± 1.2	1.0 ± 0.2	0.60 ± 0.05	1.24

[a] All at 37 °C, except for EZRDM at 30 °C [19].
[b] From initial slope of MSD plots (Fig. 2A).
[c] Best-fit parameters from two-state fitting of $P_{EF\text{-}Tu}(r)$ histograms (Figs. 2B and 3B and S4B and C, and Materials and Methods). Fractional population of the fast state is $f_{fast} = (1 - f_{slow})$. χ^2_ν is the reduced chi-square statistic for the best fit.

fixes $f_{fast} = (1 - f_{slow} - f_{medium})$. The results are detailed in Table S2. The best three-state fit gave $\chi^2_\nu = 1.02$, only a marginal improvement over the best two-state fit. In all four growth conditions, two-state and three-state fits gave quite similar fractions f_{fast} and diffusion coefficients D_{fast}.

As in the earlier study of the VH1000 strain growing in EZRDM at 30 °C [19], D_{slow} is ~5 times larger than the 70S polysome diffusion coefficient of $D_{polysome} = 0.3 \pm 0.1\ \mu m^2/s$. Once again we infer that D_{slow} represents a composite diffusive state. The typical binding time of a TC to the translating ribosome is evidently shorter than one camera frame = 2 ms, so that D_{slow} represents a weighted average over a mixture of bound and free populations. In the earlier study [19], we showed that the spatial distribution of the slow population indeed mimics the three-peaked distribution of the ribosomes [36,37], most of which are translating at a given moment. Such a short binding time is consistent with the fast overall elongation rates of ~20 amino acids per second and the need to test ~40 aa-tRNAs on average to find a codon match [11,38] (see Discussion).

In the present case of MBM-glucose with 0.1 M NaCl, in order to match $D_{slow} = 1.35 \pm 0.3\ \mu m^2/s$, the slow population must be a mixture of 69% ± 13% ribosome-bound and 31% ± 13% free copies. This estimate assumes that free TCs within the ribosome-rich regions diffuse with $D_{fast} = 3.7\ \mu m^2/s$. The conclusion is that at any given moment, 46% ± 9% of the entire EF-Tu population comprises TCs bound to translating ribosomes: this is 0.69 of the 67% ± 5% of copies exhibiting the slow apparent diffusion coefficient D_{slow}.

We can leverage this result to provide a quantitative estimate of the mean number of EF-Tu copies (TCs) bound to each translating ribosome. In all conditions studied here, including MBM-glucose with 0.1 M NaCl, Hwa and others [14,16,18] have found that the total copy number of EF-Tu is six to seven times greater than the total copy number of ribosomes. In addition, for MBM-glucose with 0.1 M NaCl, only 85% ± 5% of ribosomes occur as translating 70S copies [14]. From Eq. (4) in Materials and Methods, we conclude that on average, the mean number of EF-Tu bound as TCs to each translating ribosome is $N_{EF\text{-}Tu/70S} = 3.5 \pm 0.8$. That is, the four L7/L12 stalk proteins are essentially saturated with TCs. The overall uncertainty comes from propagating uncertainties in each factor in Eq. (4).

Alternatively, we can obtain an analogous estimate of $N_{EF\text{-}Tu/70S}$ using the three-state fitting results of Table S2. Details are provided in the Materials and Methods section. Here we assume that f_{slow} arises from a population of TCs that remain ribosome-bound for the entire 2 ms frame duration, f_{medium} is a composite population that makes bound-free transitions during the 2 ms frame time, and f_{fast} arises from freely diffusing copies. For MBM with 0.1 M NaCl, the result is $N_{EF\text{-}Tu/70S} = 3.5$, the same as that obtained from the two-state fits.

Comparisons across different nutrient and osmotic conditions

For the higher salt condition MBM-glucose with 0.4 M NaCl (doubling time 104 min), $D_{Mean} = 1.79 \pm 0.16\ \mu m^2/s$ from the MSD plot (Fig. 2a), essentially the same as for 0.1 M NaCl. The distributions $P_{EF\text{-}Tu}(r)$ for the two salt conditions are compared directly in Fig. 3a, and the two-state decomposition for 0.4 M NaCl is shown in Fig. 3b. The two-state fitting procedure yields $D_{slow} = 1.0 \pm 0.1\ \mu m^2/s$, $D_{fast} = 3.5 \pm 1.0\ \mu m^2/s$, and $f_{slow} = 0.65 \pm 0.05$. The raw data and the numerical fitting results are quite similar for the two osmotic conditions, although the doubling time has increased by a factor of 1.65, from 62 min at low salt to 104 min at high salt. For glucose medium at higher salt, the same procedure yields $N_{EF\text{-}Tu/70S} = 3.9 \pm 0.6$ for the estimated number of TCs bound to each translating ribosome.

Still slower doubling times are achieved by changing the growth medium to MBM-acetate with 0.1 M or 0.4 M NaCl, resulting in doubling times of 101 and 190 min, respectively. The values of D_{Mean} from MSD plots and the best-fit two-state diffusion coefficients remain quite similar to those in glucose (Table 1). In addition, the estimated number of TCs bound to each translating ribosome remains high, $N_{EF\text{-}Tu/70S} = 3.6 \pm 0.7$ and 3.9 ± 0.7, respectively. For all these cases, the measured distributions $P_{EF\text{-}Tu}(r)$ and the best two-state fits are presented in Figs. S3 and S4. The numerical results are summarized in Tables 1 and 2.

The SI also summarizes the best three-state fits in each case. In all four growth conditions, the three-state fits yield estimates for $N_{EF\text{-}Tu/70S}$ that lie within 10% of the estimates from two-state fits. The conclusion that the four L7/L12 sites are essentially saturated with TCs under all four growth conditions is robust.

Finally, we re-state a control from the earlier study [19] that demonstrates that our analysis does not always find ~4 bound EF-Tu per 70S ribosome. There we expressed an mEos2-labeled EF-Tu^{L148A} mutant from a plasmid and measured its diffusive properties. The Rodnina lab [21] has shown that this mutation causes weaker binding to L7/L12. Accordingly, the same analysis procedure yielded the result of 1.8 bound EF-Tu^{L148A} per 70S ribosome. When mEos2-labeled WT EF-Tu was expressed from an analogous plasmid, we recovered the result of ~4 bound EF-Tu copies per 70S ribosome.

Discussion

It is important to recognize that these measurements locate and track EF-Tu copies, not TCs *per se*.

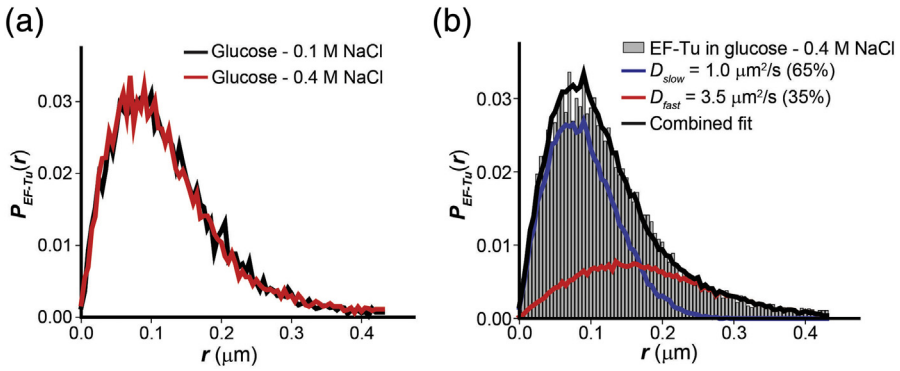

Fig. 3. (a) Comparison of experimental single-step length distributions of EF-Tu in MBM-glucose plus 0.1 M NaCl and 0.4 M NaCl. The two distributions overlap closely. (b) Best-fit two-state model of $P_{EF\text{-}Tu}(r)$ in MBM-glucose plus 0.4 M NaCl.

In live *E. coli*, EF-Tu can occur as bare EF-Tu or as EF-Tu within a charged TC (aa-tRNA–EF-Tu–GTP). In our earlier study in EZRDM, we used *in vitro* binding constants to estimate that in *E. coli* the TCs outnumber bare EF-Tu copies by about a factor of 2.2 (~70% of all EF-Tu present as TCs). Our data do not directly demonstrate that the slowly diffusing component involves TCs bound to ribosomes. *In vitro* kinetics studies have shown that both bare EF-Tu [39] and TCs [21,22,40] bind to 70S ribosomes. However, in similar conditions *in vitro*, k_{on} is about 1000 times larger for TCs [41] than for bare EF-Tu [39]. This indicates that an empty L7/L12 site will almost always capture a TC rather than a bare EF-Tu.

For a given mRNA codon waiting for arrival of a matching tRNA at the A-site, the vast majority of TCs are not cognate. We previously estimated that on average ~40 TCs must be tested before finding a cognate TC [11,38]. Thus, our measurements apply to the typical event in which a mismatched TC binds to one of the L7/L12 sites, is tested for a codon match, fails the test, and dissociates from the A-site without GTP hydrolysis becoming once again a free TC. A simple model of this process for non-cognate TCs is depicted in Fig. 1a. As suggested before [20], the presence of four flexibly tethered L7/L12 binding sites in close proximity to the A-site may serve to capture TCs efficiently and to provide a steady supply of TCs for rapid codon testing. The average translation rate in *E. coli* can be as fast as ~20 aa/s [3,42]. If 40 TCs on average must be tested before finding a codon match, the timescale for binding and testing an individual TC must be ~1 ms or faster. It may be much less if subsequent processing of a matching aa-tRNA takes up a substantial fraction of the elongation cycle. That estimate supports our assumption that the best-fit values of D_{slow} ~ 1 μm^2/s are a weighted average of diffusion while bound to the ribosome and diffusion while searching for an open L7/L12 binding site.

Across the different nutrients and different external osmolalities tested, for which the doubling time varies from 62 to 190 min, we find no significant quantitative differences in EF-Tu/TC diffusive properties. The best-fit diffusion coefficients D_{fast} of the freely diffusing component all lie in the range 3.5–4.3 μm^2/s, and they overlap each other within the error estimates (Table 1). This observation is qualitatively consistent with the results of an earlier study of GFP diffusion in the cytoplasm of *E. coli* grown in MBM with glucose as carbon source and adapted to high growth osmolality induced by addition of NaCl in the medium [43]. For cells adapted to grow at 0.28 and 0.65 Osm (nearly matching our two MBM/glucose conditions), the mean GFP diffusion coefficient was 13.8 ± 3.8 and 13.3 ± 3.2 μm^2/s, respectively. Only at higher growth osmolality did the GFP diffusion coefficient

Table 2. Number of EF-Tu bound per 70S ribosome for different growth conditions

Growth medium	$\alpha^{a,b}$	$f_{slow}{}^{a,b}$	$Q^{a,c}$d	$\beta^{a,d}$	$N^{a}_{EF\text{-}Tu/70S}$
Glucose–0.1 M NaCl	0.69 ± 0.13	0.67 ± 0.05	6.5 ± 0.5	0.85 ± 0.05	3.5 ± 0.8
Glucose–0.4 M NaCl	0.78 ± 0.08	0.65 ± 0.05	6.5 ± 0.5	0.85 ± 0.05	3.9 ± 0.6
Acetate–0.1 M NaCl	0.70 ± 0.10	0.55 ± 0.05	6.5 ± 0.5	0.70 ± 0.05	3.6 ± 0.7
Acetate–0.4 M NaCl	0.64 ± 0.08	0.65 ± 0.05	6.5 ± 0.5	0.70 ± 0.05	3.9 ± 0.7

[a] Parameters from Eq. (4).
[b] Values obtained from two-state fitting as shown in Table 1.
[c] The copy number ratio of EF-Tu to ribosome stays nearly constant across growth conditions [14,16].
[d] Values for glucose and acetate at 0.1 M NaCl are obtained from Fig. 3c of Dai et al. [14]. The values for higher salt are kept same as the lower salt according to Fig. 1d of Dai et al. [16].

begin to decrease, and the decrease remained quite moderate even up to 1.45 Osm.

In all growth conditions studied here, our results combined with copy number estimates from the literature indicate that the four L7/L12 stalk proteins on translating ribosomes are nearly saturated with TCs. The estimates for $N_{EF\text{-}Tu/70S}$ (Table 2) all lie in the narrow range 3.5–3.9 and overlap each other within the error estimates. A variety of other GTPases, most importantly EF-G, but also including factors such as IF2, EF4/LepA, and RF3, must compete with EF-Tu for L7/L12 binding sites [20,23,44,45]. Most of these factors exhibit *in vitro* binding constants to L7/L12 that are comparable to that of EF-Tu [23,46]. However, it is plausible that EF-Tu will dominate occupancy of the L7/L12 sites, primarily because of the much smaller copy numbers of its competitors. For example, in glucose minimal medium, there are 6–7 EF-Tu copies per ribosome compared with only ~1 EF-G copy per ribosome [18]. This is consistent with the fact that arrival of every aa-tRNA (cognate and non-cognate) must involve TC binding to L7/L12, whereas EF-G is needed only when a cognate TC is accommodated into the A-site, a relatively rare event. In similar growth conditions, the EF-Tu copy number exceeds those of IF2, EF4/LepA, and RF3 by a factor of 200–300 [18]. Accordingly, these factors are required only for translation initiation, back-translocation, or termination, which are extremely rare events.

Finally, the copy numbers relative to ribosomes of EF-Tu (6–7), EF-G (0.8–0.9), and tRNA (~9) remain sensibly constant across all the growth conditions studied here [14,16]. In addition, the tRNA charging levels lie in the narrow range 60%–80% [14,16]. We therefore expect the partitioning of EF-Tu copies between TCs and bare EF-Tu to be similar in all the conditions studied here. The stability of the number of bound EF-Tu per 70S ribosome across growth conditions seems consistent with that result.

The present results indicate that delivery of TCs to the L7/L12 binding sites of the translating ribosome is not the rate-limiting step in the overall translation process, at least for the range of growth conditions investigated here. This conclusion disagrees with inferences drawn in the recent work from the Hwa lab. Under nutrient limitation, they concluded that the overall translation rate decreases primarily due to a shortage of TCs [14]. Under hyperosmotic stress, they concluded that the translation rate decreases primarily due to enhanced crowding, which slows the diffusion-limited rate of binding of TCs to the ribosomal A-site [16]. The coarse-grained Michaelis–Menten model with ribosome as enzyme and cognate TCs as substrate fits the Hwa data well, but would seem to require modification.

If delivery of TCs to the L7/L12 sites is not rate limiting for the overall translation rate, what is the rate-limiting step? There are many possibilities—protein synthesis is a complex, multistep process. First the 30S subunit must find a Shine–Dalgarno sequence on a message [47]. The 50S subunit must be recruited and synthesis begun with the help of the initiation factors IF1, IF2 and IF3 [48]. Each subsequent elongation cycle involves recruitment and testing of TCs, accommodation of a codon-matched aa-tRNA at the A-site, formation of the new chemical bond to the growing peptide chain, and translocation of the message and the tRNAs through the ribosome with the help of EF-G [6]. Once the chain is complete, additional factors RF1, RF2, and RF3 assist termination [49]. Our results only indicate that one or several of these many mechanistic steps becomes slower and rate limiting under both nutrient limitation and higher growth osmolality.

One common consequence of both nutrient limitation and osmotic upshift is enhanced synthesis of the "magic spot," (p)ppGpp [50–53]. *In vitro* binding studies indicate that ppGpp competes with GTP for its binding site within many GTPases, including EF-Tu within the TC, EF-G, EF-Ts, the translation initiation factor IF2, and also the release factor RF3 [44,45,54]. A simple suggestion is that as growth slows down, one or several of these cofactors occasionally arrive at the ribosome containing ppGpp rather than GTP. For example, if a fraction of TCs contained ppGpp, it would not perturb the initial TC binding step to L7/L12, because the GTP binding site is different from the L7/L12 binding site [21,55]. However, when a cognate TC arrives at the A-site, the accommodation process is driven by activation of the GTPase within the TC, GTP hydrolysis, and phosphate release [6]. The overall translation rate would be suppressed if some fraction of the cognate TCs contained not GTP, but ppGpp, thus thwarting the accommodation step. This is only one of many possibilities.

Materials and Methods

Bacterial strains

In *E. coli*, EF-Tu is expressed from two essentially identical genes: *tufA* and *tufB.* Both of these genes were endogenously labeled at the C-terminus with a photoconvertible fluorescent protein, mEos2, *via* the lambda red technique [56] in the background strain NCM3722, the same strains used by the Hwa lab [14,16]. The doubling time of the labeled strain is 62 ± 2 min compared to 48 ± 1 min for the WT strain, when grown in MBM with glucose and normal osmolality (0.28 Osm) at 37 °C. The labeling causes a ~30% increase in doubling time, a moderate growth defect considering that EF-Tu is an essential protein. The growth conditions and the corresponding doubling times of the labeled EF-Tu strain are collected in Table S1.

Cell growth and preparation for imaging

The cells were grown in an air shaker (New Brunswick Excella E24, from Eppendorf) maintained at 200 rpm and 37 °C. Bulk cultures from frozen glycerol stock solution were grown overnight to stationary phase in LB or LB + 0.3 M NaCl. On the following day, the stationary phase culture was first washed and then again grown to stationary phase in MBM, a Mops-buffered solution with supplemental metal ions (M2101; Teknova, contains 0.05 M NaCl), glucose (0.2% w/v) or sodium acetate (60 mM), 1.32 mM KH_2PO4, and varying amounts of NaCl. The NaCl amount was varied to obtain a final Na^+ concentration of 0.1 or 0.4 M, yielding final osmolality of ~0.28 and ~0.81 Osm, respectively. Osmolalities were measured with a Wescor Vapro 5520 vapor pressure osmometer (Wescor, Logan, UT). On the following day, the stationary phase culture was divided into subcultures with 100-fold dilution in fresh MBM with appropriate NaCl concentration and grown again to exponential phase (OD = 0.2–0.5). Cells were then plated on a polylysine-coated coverslip and covered with a CoverWell perfusion chamber (Electron Microscopy Science, PA) with a well volume of 140 µL.

Superresolution imaging of live *E. coli* cells

The imaging and single-particle trajectory analysis were performed similarly to the method described in our previous study [19]. The cells were imaged within 5 min of plating. Individual fields of view were imaged no longer than 20 s to minimize laser damage. Each prepared sample was imaged for no longer than 30 min, during which cells continued to grow normally. Cells were imaged on an inverted microscope (Nikon Instruments, model Eclipse-Ti, Melville, NY) equipped with an oil immersion objective (CFI Plan Apo Lambda DM 100x Oil, 1.45 NA; Nikon Instruments), a 1.5× tube lens, and the Perfect Focus System (Nikon Instruments, Melville, NY). The fluorescence images were recorded on a back-plane illuminated electron-multiplying charge-coupled device camera (Andor Technology, iXon DV-860, South Windsor, CT) at the rate of 485 Hz (2.06 ms/frame). The camera chip consisted of 128 × 128 pixels, each 24 µm × 24 µm. The effective pixel size after 150x magnification is 0.16 µm × 0.16 µm. The fluorescent protein mEos2 was activated using a 405-nm laser (CrystalLaser, Reno, Nevada, CW laser); the photoconverted state was subsequently excited with a 561-nm laser (Coherent Inc., Sapphire CW laser, Bloomingfield, CT). Both lasers illuminated the sample for the entire duration of image acquisition. Emission was collected through a 617/73 bandpass filter (bright line 617/73-25; Semrock, Rochester, NY) or a 610/75 bandpass filter (Chroma technology Corp, Bellows Falls, VT). The 405-nm power density at the sample was ~5–10 W/cm^2, which kept the average number of activated molecules in each camera frame to ~1. The 561-nm laser power density at the sample was ~8 kW/cm^2.

Single-molecule image analysis

The fluorescence images were analyzed using a MATLAB GUI developed in our lab. Two different digital filters were used to attenuate the noise in the images, namely, Gaussian and boxcar. Fluorescent signals were then identified using a peak finding algorithm with a user-defined single-pixel intensity threshold. A particle is identified if the local intensity maximum is higher than the threshold. The threshold is carefully chosen large enough so that the algorithm can distinguish between the background and the signal and small enough to avoid cutting trajectories unduly short.

A centroid algorithm was used to locate the identified particles with sub-pixel resolution. Rapidly moving molecules have images that are blurred asymmetrically due to diffusion during the camera frame. Centroid fitting can locate these particles with better accuracy than Gaussian fitting. The centroid algorithm is also faster computationally. A 7 × 7 pixel box was drawn around the intensity maxima, and the centroid of all the pixel intensities within the box was calculated. The centroid positions from successive frames were connected to form a trajectory only if they lie within 3 pixel = 480 nm of each other. A modified MATLAB version of the tracking program written by Crocker and Grier was used [57].

Mean-square displacement plots MSD(τ)

The mean-square displacement (MSD) as a function of lag time τ provides a measure of the mean diffusion coefficient averaged over all molecules. It is defined by $MSD(\tau) = \langle (\boldsymbol{r}(t+\tau) - \boldsymbol{r}(t))^2 \rangle$, where $\boldsymbol{r}(t)$ is the two-dimensional location of the particle at time t, τ is the lag time, and the average is taken over all times t and over many trajectories. The slope of the first two points of an MSD(τ) plot provides an estimate of the mean diffusion coefficient: D_{Mean} = slope/4. The MSD equation factors in the localization error σ, which can be measured from the y-intercept of the plot [58], but it does not account for confinement effects. Even for six-step-long (12 ms) trajectories, for rapidly diffusing species with $D \sim 5\ \mu m^2\ s^{-1}$, confinement restricts diffusive trajectories and causes downward curvature of the MSD plot. Hence, the estimated mean diffusion coefficient yields a lower bound of the true D_{Mean}. The trajectory analysis presented below takes into account both the localization error and confinement effects.

Monte Carlo simulations of diffusive trajectories

As explained in our previous work [19,34], we fit our experimental $P_{\text{EF-Tu}}(r)$ single-step displacement distribution with two-state simulated distributions that account for the confinement effects. There is no analytical solution that includes confinement effects; the best estimates of the true diffusion coefficients are obtained by simulation. We have assumed that the two diffusive states have different localization errors, σ_{slow} and σ_{fast}. The estimation of σ_{slow} and σ_{fast} is explained in detail in our previous paper [19].

We simulated large number of random walk trajectories, each moving with a particular diffusion coefficient D with localization error σ_{slow} or σ_{fast}. The simulations are carried out in a confining spherocylinder, which mimics the mean length of an *E. coli* cell growing in each particular growth medium. The cell diameter was kept at 0.8 μm, consistent with the observation from phase contrast imaging that cell diameter varies little under different growth conditions. Each set of simulated trajectories represents one diffusive state with fixed D and σ. We simulated 5000 six-step long trajectories for each set, with 1000 microsteps during the 2 ms time between camera frames. These trajectories are used to compute model-based, numerical one-step probability distributions $P_{\text{model}}(r;D)$ for the numerical least-squares analysis of the corresponding experimental distributions. The simulation procedure is explained in more detail in our previous paper [19].

Fitting of single-step $P(r)$ distributions to static, two-state models

For every growth condition, experimental trajectories that lasted six steps or longer were selected for analysis. The trajectories were truncated at the sixth step. The six-step trajectories were then sliced into individual steps. The displacement in every step was calculated as $r_i = \sqrt{(x_{i+1}-x_i)^2 + (y_{i+1}-y_i)^2}$ and was pooled to form the distribution $P(r)$ as in Fig. 2b. We typically attempt to fit the experimental distribution $P(r)$ in a least-squares sense to a weighted average of two static populations. For unconstrained models including two static (non-exchanging) states, the fitting function is the linear combination $P_{\text{model}}(r) = f_{\text{slow}}P(r;D_{\text{slow}}) + (1 - f_{\text{slow}})P(r;D_{\text{fast}})$. Here the three fitting parameters are D_{fast}, D_{slow}, and the fractional population f_{slow}, which in turn fixes $f_{\text{fast}} = (1 - f_{\text{slow}})$. For all our fitting procedures, D_{fast} ranged from 0.1 to 9 μm^2/s with interval of 0.1 μm^2/s and D_{slow} ranged from 0.05 to 3 μm^2/s with interval of 0.05 μm^2/s. The goodness of each fit was evaluated by calculating the reduced chi-square statistic (χ_U^2). We generated a 3-D matrix of χ_U^2 values, with each axis representing one of the three fitting parameters. The parameters which gave the minimum χ_U^2 were chosen as the best fit. The $P(r)$ fitting and the error estimation in the fitting parameters are explained in further detail in our previous paper [19]. The fitting results for each of the growth conditions are listed in Table 1.

Average number of copies of EF-Tu bound to one translating, 70S ribosome

Two-state modeling of the single-step displacement distribution $P_{\text{EF-Tu}}(r)$ yields the best fit parameters D_{fast}, D_{slow}, and f_{slow} plus their uncertainties. In all cases, D_{slow} is much larger than the diffusion coefficient of translating, 70S ribosomes, D_{70S} = 0.3 ± 0.1 μm^2/s. Therefore, we assert that D_{slow} is a weighted average of the 70S diffusion coefficient and of D_{fast}:

$$D_{\text{slow}} = \alpha D_{70S} + (1-\alpha) D_{\text{fast}}, \tag{2}$$

where α is the fraction of the apparent slow population that is bound to 70S ribosomes. We can solve for α in terms of measured quantities:

$$\alpha = (D_{\text{fast}} - D_{\text{slow}})/(D_{\text{fast}} - D_{\text{Rb}}) \tag{3}$$

The mean number of EF-Tu copies bound per 70S ribosome is then:

$$N_{\text{EF-Tu/70S}} = \frac{\alpha f_{\text{slow}} Q}{\beta}, \tag{4}$$

where f_{slow} is the apparent fraction of slow EF-Tu copies, Q is the ratio of total EF-Tu copies to total ribosome copies, and β is the fraction of ribosomes engaged in translation. For all growth conditions studied here, Q lies in the range 6–7 and β (for glucose) = 0.85 ± 0.05 and β (for acetate) = 0.70 ± 0.05. The values for the 0.1 M NaCl media for both glucose and acetate are obtained from Ref. [14]. The values for higher salt media are kept same as the lower salt ones in accord with Ref. [16]. Table 2 includes the values of α, Q, and β used for each of the four growth conditions studied, along with their estimated uncertainties. The resulting values of $N_{\text{EF-Tu/70S}}$ are included in Table 2 in the main text. The uncertainties are derived by propagating uncertainties in each of the factors in Eq. (4).

For three-state fitting (Table S3), the analogous equations are:

$$N_{\text{EF-Tu/70S}} = (\alpha f_{\text{medium}} + f_{\text{slow}}) Q/\beta \tag{5}$$

$$\alpha = (D_{\text{fast}} - D_{\text{medium}})/(D_{\text{fast}} - D_{\text{slow}}) \tag{6}$$

The resulting values are included in Table S2.

Acknowledgments

We thank Prof. Terence Hwa (University of California-San Diego) for help in preparing the strains used in this study. In addition, Prof. Hwa first suggested that we study EF-Tu diffusion. We also acknowledge Dr. Soni Mohapatra and Dr. Heejun Choi for many fruitful scientific discussions and for suggestions for improving the analysis of the diffusion data.

This work was supported by the National Science Foundation (MCB-1512946 to J.C.W.) and by the National Institutes of Health (NIGMS, R01-GM094510 to J.C.W.). The content is solely the responsibility of the authors and does not necessarily represent the official views of the National Institutes of Health.

Appendix A. Supplementary data

Supplementary data to this article can be found online at https://doi.org/10.1016/j.jmb.2019.04.037.

Received 17 January 2019;
Received in revised form 26 March 2019;
Accepted 21 April 2019
Available online 30 April 2019

Keywords:
nutrient limitation;
high osmolality;
superresolution microscopy;
ternary complex;
diffusion

Abbreviations used:
EF-Tu, elongation factor-Tu; aa-tRNA, aminoacyl-tRNA; TC, ternary complex; WT, wild type; MBM, MOPS-based minimal medium.

References

[1] H. Bremer, P. Dennis, Modulation of chemical composition and other parameters of the cell at different exponential growth rates, EcoSal Plus (2008)https://doi.org/10.1128/ecosal.5.2.3.
[2] D.G. Dalbow, R. Young, Synthesis time of beta-galactosidase in *Escherichia coli* B/r as a function of growth rate, Biochem. J. 150 (1975) 13–20.
[3] R. Young, H. Bremer, Polypeptide-chain-elongation rate in *Escherichia coli* B/r as a function of growth rate, Biochem. J. 160 (1976) 185.
[4] S.H. Li, Z. Li, J.O. Park, C.G. King, J.D. Rabinowitz, N.S. Wingreen, et al., *Escherichia coli* translation strategies differ across carbon, nitrogen and phosphorus limitation conditions, Nat. Microbiol. 3 (2018) 939–947.
[5] F.C. Neidhardt, B. Magasanik, Studies on the role of ribonucleic acid in the growth of bacteria, Biochim. Biophys. Acta 42 (1960) 99–116.
[6] R.M. Voorhees, V. Ramakrishnan, Structural basis of the translational elongation cycle, Annu. Rev. Biochem. 82 (2013) 203–236.
[7] I. Wohlgemuth, C. Pohl, J. Mittelstaet, A.L. Konevega, M.V. Rodnina, Evolutionary optimization of speed and accuracy of decoding on the ribosome, Philos. Trans. R. Soc. Lond. Ser. B Biol. Sci. 366 (2011) 2979–2986.
[8] T. Pape, W. Wintermeyer, M.V. Rodnina, Complete kinetic mechanism of elongation factor Tu-dependent binding of aminoacyl-tRNA to the A site of the *E. coli* ribosome, EMBO J. 17 (1998) 7490–7497.
[9] S.C. Blanchard, R.L. Gonzalez, H.D. Kim, S. Chu, J.D. Puglisi, tRNA selection and kinetic proofreading in translation, Nat. Struct. Mol. Biol. 11 (2004) 1008–1014.
[10] P. Geggier, R. Dave, M.B. Feldman, D.S. Terry, R.B. Altman, J.B. Munro, et al., Conformational sampling of aminoacyl-tRNA during selection on the bacterial ribosome, J. Mol. Biol. 399 (2010) 576–595.
[11] S. Rudorf, M. Thommen, M.V. Rodnina, R. Lipowsky, Deducing the kinetics of protein synthesis in vivo from the transition rates measured in vitro, PLoS Comput. Biol. 10 (2014), e1003909.
[12] S. Rudorf, R. Lipowsky, Protein synthesis in *E. coli*: dependence of codon-specific elongation on tRNA concentration and codon usage, PLoS One 10 (2015), e0134994.
[13] G. Zhang, I. Fedyunin, O. Miekley, A. Valleriani, A. Moura, Z. Ignatova, Global and local depletion of ternary complex limits translational elongation, Nucleic Acids Res. 38 (2010) 4778–4787.
[14] X. Dai, M. Zhu, M. Warren, R. Balakrishnan, V. Patsalo, H. Okano, et al., Reduction of translating ribosomes enables *Escherichia coli* to maintain elongation rates during slow growth, Nat. Microbiol. 2 (2016), 16231.
[15] S. Klumpp, M. Scott, S. Pedersen, T. Hwa, Molecular crowding limits translation and cell growth, Proc. Natl. Acad. Sci. U. S. A. 110 (2013) 16754–16759.
[16] X. Dai, M. Zhu, M. Warren, R. Balakrishnan, H. Okano, J.R. Williamson, et al., Slowdown of translational elongation in *Escherichia coli* under hyperosmotic stress, mBio 9 (2018), e02375-02317.
[17] F.C. Neidhardt, P.L. Bloch, S. Pedersen, S. Reeh, Chemical measurement of steady-state levels of ten aminoacyl-transfer ribonucleic acid synthetases in *Escherichia coli*, J. Bacteriol. 129 (1977) 378–387.
[18] A. Schmidt, K. Kochanowski, S. Vedelaar, E. Ahrne, B. Volkmer, L. Callipo, et al., The quantitative and condition-dependent *Escherichia coli* proteome, Nat. Biotechnol. 34 (2016) 104–110.
[19] M. Mustafi, J.C. Weisshaar, Simultaneous binding of multiple EF-Tu copies to translating ribosomes in live *Escherichia coli*, mBio 9 (2018), e02143-02117.
[20] M. Diaconu, U. Kothe, F. Schlunzen, N. Fischer, J.M. Harms, A.G. Tonevitsky, et al., Structural basis for the function of the ribosomal L7/12 stalk in factor binding and GTPase activation, Cell 121 (2005) 991–1004.
[21] U. Kothe, H.J. Wieden, D. Mohr, M.V. Rodnina, Interaction of helix D of elongation factor Tu with helices 4 and 5 of protein L7/12 on the ribosome, J. Mol. Biol. 336 (2004) 1011–1021.
[22] R.R. Traut, D. Dey, D.E. Bochkariov, A.V. Oleinikov, G.G. Jokhadze, B. Hamman, et al., Location and domain structure of *Escherichia coli* ribosomal protein L7/L12: site specific

cysteine crosslinking and attachment of fluorescent probes, Biochem. Cell Biol. 73 (1995) 949–958.
[23] M. Helgstrand, C.S. Mandava, F.A. Mulder, A. Liljas, S. Sanyal, M. Akke, The ribosomal stalk binds to translation factors IF2, EF-Tu, EF-G and RF3 via a conserved region of the L12 C-terminal domain, J. Mol. Biol. 365 (2007) 468–479.
[24] A. Liljas, S. Sanyal, The enigmatic ribosomal stalk, Q. Rev. Biophys. 51 (2018) e12.
[25] E. Betzig, G.H. Patterson, R. Sougrat, O.W. Lindwasser, S. Olenych, J.S. Bonifacino, et al., Imaging intracellular fluorescent proteins at nanometer resolution, Science 313 (2006) 1642–1645.
[26] S. Manley, J.M. Gillette, G.H. Patterson, H. Shroff, H.F. Hess, E. Betzig, et al., High-density mapping of single-molecule trajectories with photoactivated localization microscopy, Nat. Methods 5 (2008) 155–157.
[27] A.V. Furano, The elongation factor Tu coded by the *tufA* gene of *Escherichia coli* K-12 is almost identical to that coded by the *tufB* gene, J. Biol. Chem. 252 (1977) 2154–2157.
[28] O. Wiborg, C. Andersen, C.R. Knudsen, B.F.C. Clark, J. Nyborg, Mapping *Escherichia coli* elongation factor Tu residues involved in binding of aminoacyl-tRNA, J. Biol. Chem. 271 (1996) 20406–20411.
[29] B.P. English, V. Hauryliuk, A. Sanamrad, S. Tankov, N.H. Dekker, J. Elf, Single-molecule investigations of the stringent response machinery in living bacterial cells, Proc. Natl. Acad. Sci. U. S. A. 108 (2011) E365–E373.
[30] A. Nenninger, G. Mastroianni, C.W. Mullineaux, Size dependence of protein diffusion in the cytoplasm of *Escherichia coli*, J. Bacteriol. 192 (2010) 4535–4540.
[31] S. Bakshi, B.P. Bratton, J.C. Weisshaar, Subdiffraction-limit study of Kaede diffusion and spatial distribution in live *Escherichia coli*, Biophys. J. 101 (2011) 2535–2544.
[32] N. Ban, B. Freeborn, P. Nissen, P. Penczek, R.A. Grassucci, R. Sweet, et al., A 9 Å resolution x-ray crystallographic map of the large ribosomal subunit, Cell 93 (1998) 1105–1115.
[33] W.M. Clemons, J.L.C. May, B.T. Wimberly, J.P. McCutcheon, M.S. Capel, V. Ramakrishnan, Structure of a bacterial 30S ribosomal subunit at 5.5 Å resolution, Nature 400 (1999) 833–840.
[34] S. Mohapatra, H. Choi, X. Ge, S. Sanyal, J.C. Weisshaar, Spatial distribution and ribosome-binding dynamics of EF-P in live *Escherichia coli*, mBio 8 (2017) e00300–e00317.
[35] A. Sanamrad, F. Persson, E.G. Lundius, D. Fange, A.H. Gynnå, J. Elf, Single-particle tracking reveals that free ribosomal subunits are not excluded from the *Escherichia coli* nucleoid, Proc. Natl. Acad. Sci. U. S. A. 111 (2014) 11413–11418.
[36] S. Bakshi, A. Siryaporn, M. Goulian, J.C. Weisshaar, Super-resolution imaging of ribosomes and RNA polymerase in live *Escherichia coli* cells, Mol. Microbiol. 85 (2012) 21–38.
[37] Q. Chai, B. Singh, K. Peisker, N. Metzendorf, X. Ge, S. Dasgupta, et al., Organization of ribosomes and nucleoids in *Escherichia coli* cells during growth and in quiescence, J. Biol. Chem. 289 (2014) 11342–11352.
[38] H. Dong, L. Nilsson, C.G. Kurland, Co-variation of tRNA abundance and codon usage in *Escherichia coli* at different growth rates, J. Mol. Biol. 260 (1996) 649–663.
[39] R.C. Thompson, D.B. Dix, A.M. Karim, The reaction of ribosomes with elongation factor Tu.GTP complexes. Aminoacyl-tRNA-independent reactions in the elongation cycle determine the accuracy of protein synthesis, J. Biol. Chem. 261 (1986) 4868–4874.
[40] H. Stark, M.V. Rodnina, J. Rinke-Appel, R. Brimacombe, W. Wintermeyer, M.v. Heel, Visualization of elongation factor Tu on the *Escherichia coli* ribosome, Nature 389 (1997) 403–406.
[41] M.V. Rodnina, T. Pape, R. Fricke, L. Kuhn, W. Wintermeyer, Initial binding of the elongation factor Tu·GTP·aminoacyl-tRNA complex preceding codon recognition on the ribosome, J. Biol. Chem. 271 (1996) 646–652.
[42] P.P. Dennis, H. Bremer, Differential rate of ribosomal protein synthesis in *Escherichia coli* B/r, J. Mol. Biol. 84 (1974) 407–422.
[43] M.C. Konopka, K.A. Sochacki, B.P. Bratton, I.A. Shkel, M.T. Record, J.C. Weisshaar, Cytoplasmic protein mobility in osmotically stressed *Escherichia coli*, J. Bacteriol. 191 (2009) 231–237.
[44] P. Milon, E. Tischenko, J. Tomsic, E. Caserta, G. Folkers, A. La Teana, et al., The nucleotide-binding site of bacterial translation initiation factor 2 (IF2) as a metabolic sensor, Proc. Natl. Acad. Sci. U. S. A. 103 (2006) 13962–13967.
[45] A.M. Rojas, M. Ehrenberg, S.G. Andersson, C.G. Kurland, ppGpp inhibition of elongation factors Tu, G and Ts during polypeptide synthesis, Mol. Gen. Genet. 197 (1984) 36–45.
[46] A. Savelsbergh, D. Mohr, B. Wilden, W. Wintermeyer, M.V. Rodnina, Stimulation of the GTPase activity of translation elongation factor G by ribosomal protein L7/12, J. Biol. Chem. 275 (2000) 890–894.
[47] J. Shine, L. Dalgarno, The 3′-terminal sequence of *Escherichia coli* 16S ribosomal RNA: complementarity to nonsense triplets and ribosome binding sites, Proc. Natl. Acad. Sci. U. S. A. 71 (1974) 1342–1346.
[48] B.S. Laursen, H.P. Sørensen, K.K. Mortensen, H.U. Sperling-Petersen, Initiation of protein synthesis in bacteria, Microbiol. Mol. Biol. Rev. 69 (2005) 101.
[49] M. Ehrenberg, V. Dincbas, D. Freistroffer, V. Heurgué-Hamard, R. Karimi, M. Pavlov, et al., Mechanism of bacterial translation termination and ribosome recycling, in: R. Garret, S.R. Douthwaite, A. Liljas, A.T. Matheson, P.B. Moore, H.F. Noller (Eds.), The Ribosome: Structure, Function, Antibiotics and Cellular Interactions, American Society of Microbiology, Washington, DC 2000, pp. 541–551.
[50] U. Kanjee, K. Ogata, W.A. Houry, Direct binding targets of the stringent response alarmone (p)ppGpp, Mol. Microbiol. 85 (2012) 1029–1043.
[51] R.B. Harshman, H. Yamazaki, MS I accumulation induced by sodium chloride, Biochemistry 11 (1972) 615–618.
[52] K. Braeken, M. Moris, R. Daniels, J. Vanderleyden, J. Michiels, New horizons for (p)ppGpp in bacterial and plant physiology, Trends Microbiol. 14 (2006) 45–54.
[53] K. Shimizu, Regulation systems of bacteria such as *Escherichia coli* in response to nutrient limitation and environmental stresses, Metabolites 4 (2013) 1–35.
[54] B. Wang, P. Dai, D. Ding, A. Del Rosario, R.A. Grant, B.L. Pentelute, et al., Affinity-based capture and identification of protein effectors of the growth regulator ppGpp, Nat. Chem. Biol. (2018) https://doi.org/10.1038/s41589-018-0183-4.
[55] M. Kjeldgaard, P. Nissen, S. Thirup, J. Nyborg, The crystal structure of elongation factor EF-Tu from *Thermus aquaticus* in the GTP conformation, Structure 1 (1993) 35–50.
[56] L.C. Thomason, J.A. Sawitzke, X. Li, N. Costantino, D.L. Court, Recombineering: genetic engineering in bacteria using homologous recombination, Curr. Protoc. Mol. Biol. 106 (2014) (1.16.11-39).
[57] J.C. Crocker, D.G. Grier, Methods of digital video microscopy for colloidal studies, J. Colloid Interface Sci. 179 (1996) 298–310.
[58] X. Michalet, Mean square displacement analysis of single-particle trajectories with localization error: Brownian motion in an isotropic medium, Phys. Rev. E Stat. Nonlinear Soft Matter Phys. 82 (2010), 041914.